Proceedings of the International Conference on Industrial Engineering and Operations Management

Publisher: IEOM Society International, USA DOI: 10.46254/BA08.20250237
Published: December 20, 2025

CFD Analysis of the Effect of Plain Flap Deflection on NACA 2415 with A Leading-Edge Slat at Different Angles of Attack

Tahmina Kabir and Md. Mahmudul Islam
Aeronautical Engineering, MIST, Dhaka-1216, Bangladesh
nourinkabir6@gmail.com, mi.mahmud77@gmail.com

Samia Akter
Mechanical Engineering, MIST, Dhaka-1216, Bangladesh
samia.akter.ae@gmail.com

Md Amirul Islam
Mechanical Engineering, University of North Dakota, Grand Forks, ND, USA
amirul.islamhs@gmail.com

Abstract

The importance of designing a more proficient airfoil with an effective flap and slat to increase lift force, reduce stall formation, or delay flow separation has become one of the main concerns of aerodynamicists. Considering that fact, a multi-element airfoil NACA-2415 with NACA-22 leading-edge slat at a specific 25˚ angle and a plain flap with three angle deflections (0˚, 15˚, 30˚) have been studied in this work. The outcome of varied deflections of the plain flap with various Angles of Attack (AOA) has been scrutinized. This paper also specifies the critical AOA and C_{Lmax} for the multi-element airfoil's flap deflection. The entire analysis involves 2D modeling and computational fluid dynamics (CFD) simulations conducted at a high Reynolds number.

1. Introduction

Any shape of a body or particles that fly in the air is the subject of aerodynamics. But the important part is how effectively and efficiently it can fly, consuming the lowest amount of energy. An aerodynamically efficient shape ensures the best possible flight profile by providing an increased amount of lift and, at the same time, minimum drag force. That is why designers select an effective airfoil and some high-lift devices like flaps, slats, and so on to attain a higher coefficient of lift (C_L) and lower coefficient of drag (C_D).

In addition, Reynolds number (Re) plays a vital role in aerodynamic characteristics, which helps to understand the flow pattern. Re affects the airflow attachment quality, which might have a major or minor effect on some drag types. However, airfoil behaves differently with/without high lift devices, at a Re with varied Angle of Attack (AOA). Designers are conducting research to find the most suitable combination of airfoil configurations to meet their desired objectives.

In previous studies, Ahmed et al. (2023) analyzed the aerodynamic properties of a NACA 0012 airfoil with plain flaps under various flap angles and Mach numbers using simulation. When operating under various conditions with an increasing Mach number (M); lift coefficients (C_L), drag coefficients (C_D), and C_L/C_D ratio calculations were also discussed in their study. Kumar and Kumar (2013) investigated the impact of a typical plain flap with a NACA 0012 airfoil on the increasing lift during crucial flying periods at low speed with variable AOA. On the other hand, Todorov

(2015) investigated the effects of a single plain flap on the NACA 23012 airfoil's performance at 3×10^6 Re. He found that the deflection of the flap enhances the lift coefficient by almost 30% over varying AOA. He also investigated the max AOA is 12˚ in the case of deflected flaps and 18˚ in the case of baseline airfoils. Genç et al. (2009) discussed the impact of the leading-edge slat on the NACA 2415's aerodynamic coefficients and boundary layer characteristics at transitional Re. A. Prabhakar and Ohri (2013) examined the impact of the slot size and double-slotted flaps on C_L for a MAV NACA 2412 at 2×10^5 Re. They also analyzed the maximum value of C_L to be 67.134% higher than the plain NACA 2412 wing. The stall angle was increased by 34˚ compared to the baseline airfoil in the high lift take-off configuration. Arra et al. (2021) discussed the optimization of high-lift devices such as leading-edge slats and trailing-edge slotted flaps for NACA 2412. They analyzed that the multi-element NACA 2412 has good aerodynamic performance, and their obtained results have an accuracy of 1.09% for the maximum coefficient of lift and 0.4% for landing conditions. NACA 2415 airfoil was analyzed with its four types of designs for a 3-D wing of commercial aircraft and found that the wing with modified profile (root) & dihedral angle shows both the highest value of C_L and C_L/C_D ratio as compared to other designs Jain et al. (2016). They used NACA 2415 airfoil for its higher C_L/C_D ratio at low Re and Mach number. In addition, multi-element airfoil or flapped wings were simulated for several flight conditions varying their flap deflection angles, the AOA to acquire better aerodynamic characteristics (Didwania and Khatri, 2019; Anılır and Kurtuluş, 2023). Moreover, the effects of different types of flaps, their intermediate gaps, and their overlap with base airfoil were analyzed at various AOA by ANSYS Fluent (Hussein et al., 2021; Narsipur et al., 2012).

From the literature, we have seen that symmetric airfoils have been used in most plain flap studies. However, in the case of asymmetric airfoil studies, different flaps received much more analysis than just plain flaps. On the contrary, the least amount of work has been done on the multi-element configuration of the asymmetric airfoil, particularly with plain flap deflection.

In this paper, we, therefore, investigate the impact of plain flap deflection at different angles of attack on NACA 2415 with a leading-edge slat. Since NACA 2415 can generate lift at zero AOA, we classify it as an asymmetric airfoil. Given the complicated geometry of the NACA 2415 multi-element configuration, we focused on the plain flap, the most basic type of flap for our analysis. In our study, we only take the 2D analysis into account. Our study's primary goal is to observe how C_L changes as AOA varies for three flap deflection angles (0˚, 15˚, and 30˚).

This paper is structured as follows. Section 2 describes the computational setup and methodology, encompassing the design of the 2D multi-element airfoil model, meshing approach, turbulence model selection, and the solver settings with boundary conditions. Thereafter, the simulation results are scrutinized in Section 5. Finally, we conclude with the recommendation in Section 6.

2. Simulation Setup and Modeling

2.1 Multi-Element Airfoil Design

In this study, the NACA-2415 airfoil is simulated at a high Reynolds number with a leading-edge slat and a plain flap. The chord length of the NACA 2415 airfoil is taken as 1000 mm. Therefore, the airfoil has a maximum thickness of 150 mm and a maximum camber of 20 mm— located at 400 mm from the leading edge. Considering different types of slats, its position, the gap between the slat and the airfoil, and the angle of the slat relative to the airfoil chord line M S Genç, Ü Kaynak, and G D Lock found that highly cambered airfoil, NACA 22, comparatively obtains a higher maximum lift coefficient [4]. That is why we have chosen NACA 22 airfoil with a chord length of 230 mm as a slat. The slat deflection angle is 25˚, and three different models are created for flap deflection angle $\delta_f = 0˚, 15˚, 30˚$. The slat and flap are designed in SOLIDWORKS, taking inspiration from the 3D model of the Diamond DA20-C1 aircraft from Smykla et al. (2021). Figure 1 shows the diagram of NACA 2415 with a leading-edge slat and a plain flap with a deflection angle $\delta_f = 0˚$.

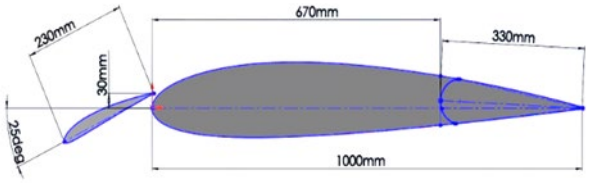

Figure 1. NACA 2415 airfoil with LE slat and TE plain flap

2.2 Turbulence Modeling

The simulation was done in ANSYS software that performed flow simulation based on Navier-Stokes equations which effectively capture fluid behaviour under various forces but are challenging to solve mathematically for complex systems. To simplify CFD simulations, numerical techniques like Reynolds-averaged Navier-Stokes (RANS), Large Eddy Simulation (LES), and Direct Numerical Simulation (DNS) have been developed, where RANS is the most popular method for reducing fluid flow complexity. The Spalart-Allmaras turbulence model is one of the RANS methods that utilize a single governing kinematic equation to describe viscous eddy current flow. The model simplifies simulations with its computational efficiency and stability in adverse pressure gradient boundary layers [3]. In this study, the simulation setup used a pressure-based solver with boundary conditions, for which Spalart-Allmaras is considered most suitable.

2.3 Meshing

Meshing is a finite element analysis used in ANSYS Fluent. For this study, a triangular surface mesh—an unstructured mesh composed of triangular cell elements—was utilized. The unstructured mesh is advantageous as it takes less time to generate the mesh grids, and the size and shape of the grids are automatically adjusted according to the geometry of the model. Generally, the triangular mesh has three control points, i.e., it is like a three-dimensional triangle.

The C flow field geometry has been drawn around the airfoil section that acts as a domain and helps to set the boundary conditions for our analysis. The flow field has been used as a boundary layer for the 2D airfoil and as our configuration is complex, the simplest form for mesh domain distance is chosen. The domain dimension for the inlet is considered as 1000 mm from the leading edge of the baseline airfoil, while the outlet is positioned 2000 mm away from it. So, the new surface area has a vertical and horizontal length of 2000 mm, whereas the radius is 1000 mm. Later it was divided into small cells to form a mesh, and each cell can be considered a small control volume. Figure 2 shows the mesh which was carried out in ANSYS for this study's purposes. On top of that, for simulation purposes, all meshed models are also defined with three named selections for each needed edge- inlet, outlet, and airfoil.

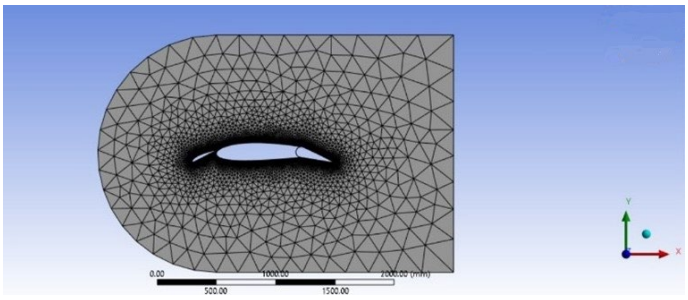

Figure 2. C flow field mesh generation of NACA 2415 multi-element airfoil

In this study, some techniques were carried out in ANSYS to increase the mesh's accuracy, which provided high refinement. The simulation uses 103,510 elements and 82,926 nodes. The inflation layers near the airfoil and slat are refined, whereas Inflation layers of 10 to 25 help resolve the boundary layer effectively, with a growth rate of 1.2. Additionally, the mesh inflation layer suggests the number of layers of cells near the wall, which is an essential parameter for simulating turbulence, especially in boundary layers. The first layer height is chosen to achieve a target y+ value around 1 with an average element size of 6.15 mm, ensuring accuracy near the airfoil and its components.

2.4 Solver Settings and Boundary Condition

In this analysis, a pressure-based solver is used, and it is assumed that the flow variables remain constant over time, indicating a steady-state simulation. The boundary conditions are defined as follows: the inlet is assigned as a velocity inlet, the outlet as a pressure outlet, and the airfoil as a solid wall with no-slip conditions. The velocity inlet is specified in terms of both magnitude and direction.

Air with a density (ρ) of 1.225 kg/m^3, a viscosity (μ) of 1.7894×10^{-5} kg/ms, and a velocity of 75 m/s (Mach 0.22) is set for the working fluid. The Reynolds number considered in this study is 5.1×10^6.

All the calculations were done for different angles of attack. The problem is initialized as hybrid initialization, and the solution is checked in the console window for convergence assurance to ensure that the simulation has reached steady-state conditions. Figure 3 shows a picture of the solver setting as an example.

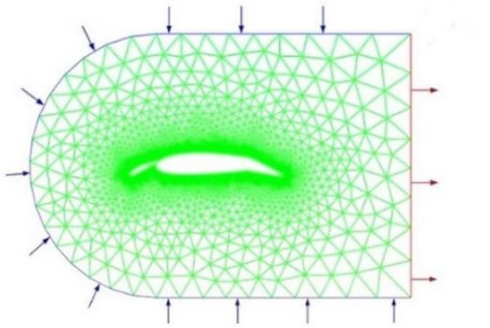

Figure 3. Mesh model in solver setting

3. Results

In this section, we present our simulation findings, i.e., C_L vs. AOA relations of NACA 2415 airfoil with 25˚ slat and varied angle flaps. We also analyze the static pressure contour and velocity contour for various configurations.

3.1 Lift Coefficient Calculations

In this study, the multi-element NACA 2415 airfoil's integrated parts– trailing-edge plain flap & leading-edge slat both increase the camber line of the airfoil. Keeping the slat fixed at 25˚deflection, we observe the influence of flap deflection and AOA variation on the coefficient of lift (C_L) values. Table 1 presents the C_L vs. AOA values for different NACA 2415 configurations. It is evident that the maximum C_L at critical AOA of flap deflection 0˚, 15˚, and 30˚ over the baseline airfoil NACA 2415 without slat and flap increases by 20%, 58%, and 85%, respectively.

Table 1. Table of C_L values for different configurations

NACA 2415 Configurations	C_L at different AOA				
	0˚	4˚	8˚	12˚	Critical AOA
No slat and flap	0.185	0.547	1.038	1.367	1.567
Slat and 0˚ flap	0.216	0.578	1.097	1.497	1.894
Slat and 15˚ flap	0.681	1.25	1.699	2.099	2.474
Slat and 30˚ flap	1.173	1.735	2.196	2.572	2.899

The simulation result proves that the multi-element configuration of the airfoil significantly improves C_L compared to a baseline NACA 2415. Naturally, the C_L increases with the increase of the AOA. A slight increment of C_L is visible between the multi-element airfoil with 0˚ flap deflection & the baseline airfoil. But for 15˚ and 30˚ flap deflection configurations, a fast rate of increment in the value of C_L is observed. From the above table, it is also visible that the highest C_{Lmax} can be found for 30˚ flap deflection configuration.

Figure 4 depicts comparative analysis. The leading-edge slat increases a small amount of camber line but significantly improves the critical AOA or stall angle. It is visible that all the multi-element airfoil models with the slat help to postpone stall formation more than the single airfoil. In our study, we got the highest critical AOA for the lowest flap deflection $\delta_f = 0^\circ$.

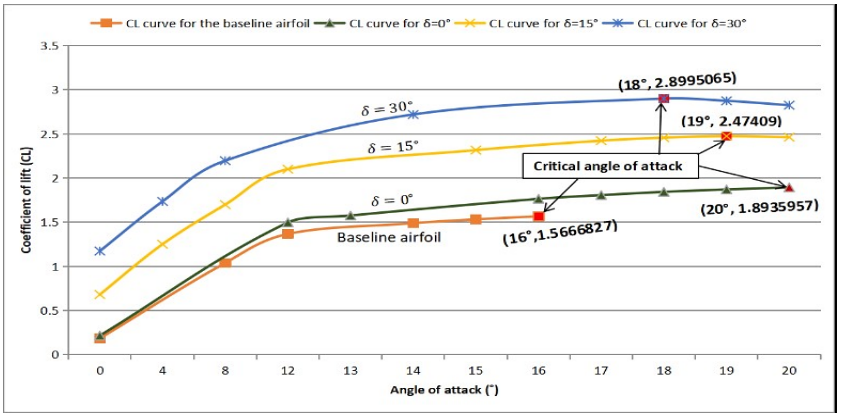

Figure 4. C_L vs. AOA of NACA 2415 airfoil with slat and flap for various configurations

We can infer from the results that, with increasing AOA, when compared to the baseline NACA 2415 airfoil, the multi-element NACA 2415 airfoil delays stalling or increases critical AOA, and with the presence of plain flap and its deflection gives tremendous increment in C_L values.

3.2 Static Pressure Contour and Velocity Contours of NACA 2415 airfoil

The multi-element configurations of airfoil exhibit significant pressure and velocity variation between the upper surface and lower surface even at zero AOA. Figure 5 to Figure 8 depicts the velocity contour, and Figure 9 to Figure 12 illustrates the static pressure contour for various airfoil configurations.

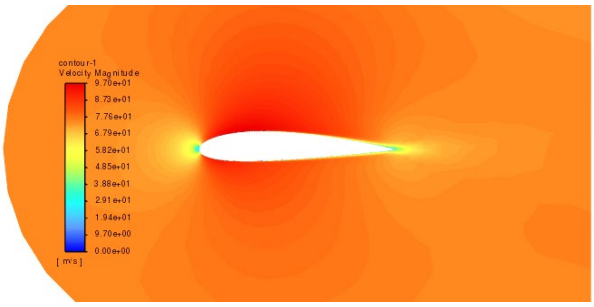

Figure 5. Velocity magnitude of NACA 2415 airfoil without slat and flap

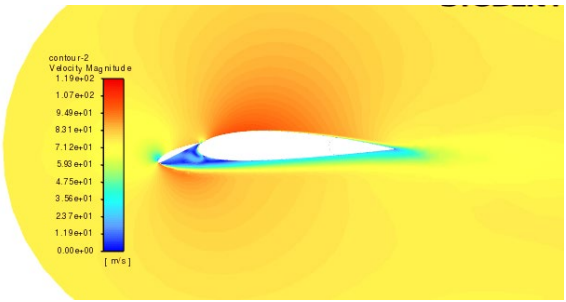

Figure 6. Velocity magnitude of NACA 2415 airfoil at 0˚ plain flap deflection

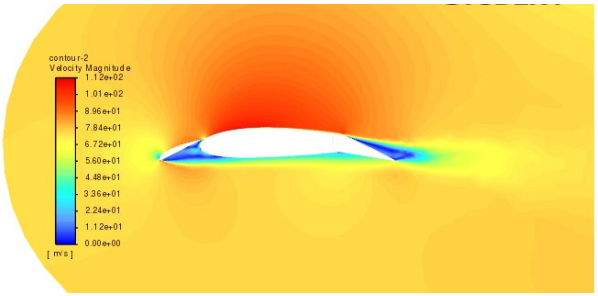

Figure 7. Velocity magnitude of NACA 2415 airfoil at 15˚ plain flap deflection

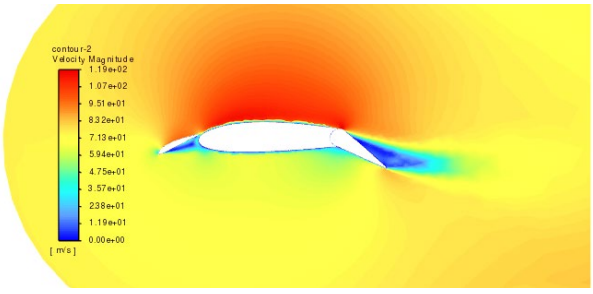

Figure 8. Velocity magnitude of NACA 2415 airfoil at 30˚ plain flap deflection

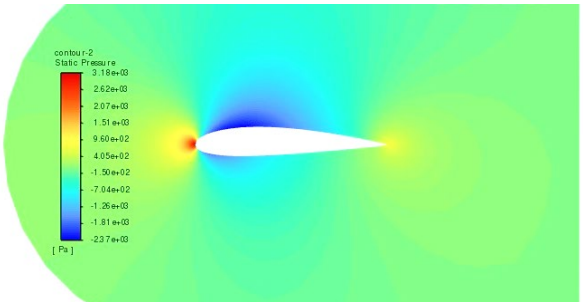

Figure 9. Static pressure contour of NACA 2415 airfoil without slat and flap

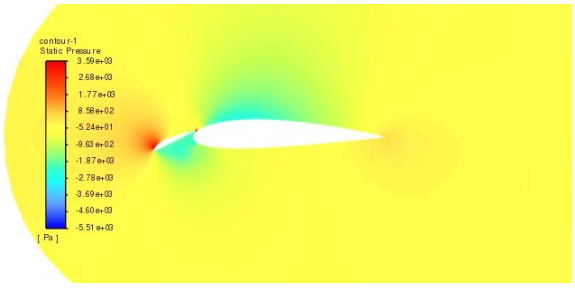

Figure 10. Static pressure contour of NACA 2415 airfoil at 0˚ plain flap deflection

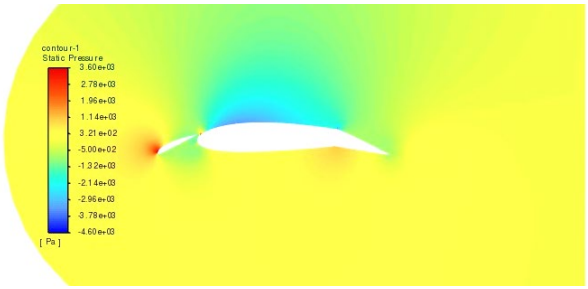

Figure 11. Static pressure contour of NACA 2415 airfoil at 15˚ plain flap deflection

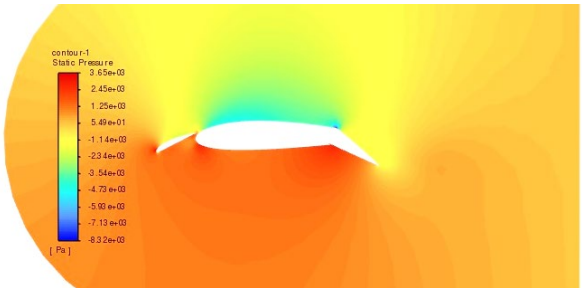

Figure 12. Static pressure Contour of NACA 2415 airfoil at 30˚ plain flap deflection

As shown by the velocity magnitude contour plots, the magnitude of the velocity in Figure 5 shows very small differences in velocity magnitude between the upper and lower camber regions of the airfoil. But in Figure 6 to Figure 8, for the multi-body system, the magnitude of velocity decreases near the lower camber region. These changes are very apparent as the flap deflection angle increases. These velocity differences between the upper and lower sides of the configuration can be very clearly visible in the leading-edge slat section and trailing-edge flap section. The slat element implies that the oncoming flow will remain laminar at greater air speeds, which will result in the creation of boundary layer transitions occurring at large AOA.

On the other hand, it is evident from the pressure contour figures, Figure 9 to Figure 12, the space between the slat and the main element guarantees pressure recovery at the leading-edge of the main element. It is also observed that as the flap deflection rises, the difference in pressure between the top and bottom surfaces also rises, which increases lift coefficients. Compared with the slat-less configuration, the value of C_L is retained for higher AOA in the case of a leading-edge slat airfoil. It happens because the slat tends to recover the flow to prevent the stall by injecting airflow through the gap between the slat and the leading-edge of the airfoil.

The multi-element structure of NACA 2415 with 15˚ flap deflection shows its C_{Lmax} at 19˚ AOA. Figure 13 and Figure 14 below illustrate the pressure and velocity contour at critical AOA.

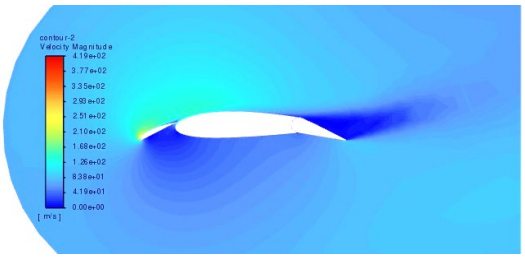

Figure 13. Velocity magnitude of NACA 2415 airfoil at 15˚ plain flap deflection at critical AOA 19˚

Figure 14. Static pressure contour of NACA 2415 airfoil at 15˚ plain flap deflection at critical AOA 19˚

4. Conclusion

In this study, C_L and C_D have been calculated for NACA 2415 airfoil with or without slat at diverse AOA and various flap deflections. The baseline airfoil exhibits a noticeably smaller increase in C_L values than the multi-element airfoil with flap deflection zero. Though for less flap deflection, the stalling can be postponed more effectively. The findings demonstrate that while the flap is at zero deflection angle, the C_L grows swiftly as the AOA rises. However, the effect of increasing C_L values became very apparent when the flap was deflected from 0˚ to 15˚ and 30˚.

For simple analysis, we consider the study using 2D steady-state computational fluid dynamics simulations of a multi-element existent airfoil- therefore it was strictly 2D CFD. A 3D geometry configuration can be used for further analysis. In addition, in this work, we focus on the lift and drag forces, but we have a plan to analyze the effect of the moment as well. Also, the Spalart-Allmaras method was implemented to solve the issue; however other approaches could be utilized in the future. Likewise, the unstructured mesh was employed in this investigation; structured mesh might be considered. Furthermore, other flap and slat designs, their gap and deflection angle with the main airfoil may be subject to better simulation yield and more efficient design. The concept of automatic slat deployment and control during extreme stall conditions can also be the topic of discussion in the future.

References

Ahmed, T., Amin, M. T., Islam, S. M. R. and Ahmed, S., Computational study of flow around a NACA 0012 wing flapped at different flap angles with varying Mach numbers, Global Journal of Researches in Engineering, vol. 13, no. 4, pp. 4–16, 2023.

Anılır, B. and Kurtuluş, D. F., Numerical investigation of SD7062 airfoil with single-slotted flap for different flight conditions, Progress in Computational Fluid Dynamics: An International Journal, vol. 23, no. 6, pp. 338–351, 2023.

Arra, A., Anekar, N. and Nimbalkar, S., Aerodynamic effects of leading edge slats and slotted trailing edge flaps on NACA-2412 airfoil in prospect of optimization, Materials Today: Proceedings, vol. 44, pp. 587–595, 2021.

Didwania, M. and Khatri, K. K., Analysis of stalling over flapped wing of an aeroplane by CFD code, IOSR Journal of Mechanical and Civil Engineering, vol. 16, no. 4, pp. 45–54, 2019.

Genç, M. S., Kaynak, Ü. and Lock, G. D., Flow over an aerofoil without and with a leading-edge slat at a transitional Reynolds number, Proceedings of the Institution of Mechanical Engineers, Part G: Journal of Aerospace Engineering, vol. 223, no. 3, pp. 217–231, 2009.

Hussein, E. Q., Azziz, H. N. and Rashid, F. L., Aerodynamic study of slotted flap for NACA 24012 airfoil by dynamic mesh techniques and visualization flow, Journal of Thermal Engineering, vol. 7, no. 2, pp. 230–239, 2021.

Jain, R., Jain, S. and Bajpai, L., Investigation on 3-D wing of commercial aeroplane with aerofoil NACA 2415 using CFD Fluent, International Research Journal of Engineering and Technology, vol. 3, no. 6, pp. 243–249, 2016.

Kumar, M. S. and Kumar, K. N., Design and computational studies on plain flaps, Bonfring International Journal of Industrial Engineering and Management Science, vol. 3, no. 2, pp. 33–39, 2013.

Narsipur, S., Pomeroy, B. W. and Selig, M. S., CFD analysis of multielement airfoils for wind turbines, 30th AIAA Applied Aerodynamics Conference, pp. 2781, 2012.

Prabhakar, A. and Ohri, A., CFD analysis on MAV NACA 2412 wing in high lift take-off configuration for enhanced lift generation, Journal of Aeronautics & Aerospace Engineering, vol. 2, no. 5, pp. 2–10, 2013.

Smykla, I., Kopeć, I. and Wolski, M., Analysis of the impact of trailing-edge wing flaps on the aerodynamic characteristics and performance of the Diamond DA-20 aircraft, Journal of Physics: Conference Series, vol. 1736, no. 1, pp. 012053, 2021.

Todorov, M., Aerodynamic characteristics of airfoil with single plain flap for light airplane wing, International Conference on Military Technologies (ICMT), pp. 1–6, 2015.